THE JOURNAL OF BIOLOGICAL CHEMISTRY
Vol. 269, No. 32, Issue of August 12, pp. 20441-20445, 1994
Printed in U.S.A.

Coordination and Spin State Equilibria as a Function of pH, Ionic Strength, and Protein Concentration in Oxidized Dimeric *Scapharca inaequivalvis* Hemoglobin*

(Received for publication, April 19, 1994, and in revised form, May 24, 1994)

Carla Spagnuolo, Francesca De Martino, Alberto Boffi, Denis L. Rousseau‡, and Emilia Chiancone

From the CNR Center of Molecular Biology, Department of Biochemical Sciences "A. Rossi Fanelli," University La Sapienza, 00185 Rome, Italy and ‡AT&T Bell Laboratories, Murray Hill, New Jersey 07974

The oxidized homodimeric *Scapharca inaequivalvis* hemoglobin undergoes changes in coordination and spin state as a function of pH, ionic strength, and protein concentration which have been monitored by optical absorption spectroscopy. Three species contribute to the spectra between pH 5.8 and 8.7: (i) a hexacoordinate high spin aquomet derivative, whose concentration is essentially constant over the whole pH range analyzed; (ii) a pentacoordinate high spin component which prevails at alkaline pH values, and (iii) a hexacoordinate low spin hemichrome, which is formed at acid pH. The contribution of each of the components to the observed spectra was calculated with the singular value decomposition procedure and has been described quantitatively in terms of a linkage scheme which accounts for the change in heme coordination and for the observation that the high spin to low spin transition entails dissociation into monomers. An important feature of the linkage scheme is the cooperative binding of protons to aquomet dimers. Stopped flow experiments to study the kinetics indicate that dissociation into monomers is the rate-limiting process. The unusually strong tendency of oxidized HbI to loose the heme-bound water molecule is discussed in terms of strain in the iron-proximal histidine bond.

The first study of oxidized *Scapharca inaequivalvis* HbI (1), carried out by means of parallel sedimentation velocity and optical spectroscopy experiments, demonstrated that the high spin dimeric protein undergoes a pH-dependent dissociation into a low spin monomeric hemichrome. However, the existence of two high spin components, an aquomet and a pentacoordinate species, in addition to the low spin hemichrome, has been brought out by the resonance Raman measurements described in the accompanying paper (2). The Raman data also show that the ratio of the three species depends not only on pH (in the range 5.8 to 8.3), but also on buffer ionic strength (between 0.01 and 0.1 M). These findings require a re-examination of the protein concentration, pH, and ionic strength dependence of the optical absorption spectra.

The present paper reports new optical spectroscopy measurements carried out as a function of pH, ionic strength, and protein concentration. These data have been supplemented with stopped flow and molecular weight measurements in order to correlate the relative amounts of high spin and low spin components to the reversible dissociation into monomers. The model proposed previously (1) has been modified in light of the present data to include formation of the pentacoordinate heme.

Nitrite-oxidized HbI has been used throughout this study, since Boffi *et al.* (3) observed that ferric HbI binds the ferrocyanide anion produced in the oxidation reaction tightly ($K >> 10^6$ M^{-1} at pH 6.1 in 0.01 M ionic strength buffer).

MATERIALS AND METHODS

The dimeric hemoglobin present in the red cells of the mollusc *S. inaequivalvis* was separated from the tetrameric one, purified as described in Ref. 4, and kept frozen at −80 °C. The protein concentration is expressed on a heme basis and was determined at 578 nm in the oxy state and at 556 nm in the deoxy state using the molar extinction coefficients ϵ = 14,300 and ϵ = 12,000, respectively (4).

Oxidation was obtained by addition of solid potassium nitrite to a concentrated solution of oxyhemoglobin dialyzed *versus* the desired buffer. The excess oxidant was removed by passage on a Sephadex G-25 column equilibrated with the same buffer. This method ensures complete oxidation and does not lead to binding of the oxidant to the protein (5).

Optical spectra were measured immediately after oxidation on a Cary 219 or Cary 3 spectrophotometer at 20 °C. In the experiments carried out as a function of protein concentration, the sample was diluted 2-fold at each step. Unless otherwise stated, MOPS[1]-NaOH was used at ionic strengths covering a range between 0.01 and 0.25 M.

Sedimentation velocity experiments were carried out using a Spinco model E ultracentrifuge equipped with a temperature control unit at 56,000 rpm and at 10 °C. The values of the sedimentation coefficients have been corrected to 20 °C in water using standard procedures.

Rapid mixing experiments have been carried out at 20 °C on an Applied Photophysics apparatus (Applied Photophysics Ltd., Leatherhead KT 227PB, UK) by mixing nitrite oxidized HbI ($3–4 \times 10^{-4}$ M) in 0.01 M MOPS-NaOH buffer at pH 7.5 with the desired buffer.

A Radiometer pH M64 was used for the pH measurements.

The absorption spectroscopy data were processed with Matlab (The Math Works Inc., South Natick, MA) on a 486 DX personal computer. The absorption spectra as a function of pH were processed by a singular value decomposition (SVD) algorithm which entails transformation of the data set, A, into a product of three matrices $A = USV^T$ (6), where the U columns are the orthonormal basis spectra, the V columns (eigenvectors) represent the corresponding amplitudes as a function of pH, and the diagonal matrix S (singular values) gives the relative contributions of the basis spectra to the observed signal. The processed data have been fitted according to the following scheme (Scheme I) where D_h and D_p are the dimeric hexacoordinate and pentacoordinate species, respectively, M is the monomeric hemichrome, K_2, K_3, K_5 and K_4 and K_6 refer to protonation and dissociation equilibria, respectively, and $K_1 = D_h/D_p$. The fit was carried out by a nested loop procedure in which in the first iteration the four equilibrium constants were obtained which yield the best fit to the three V columns (K_5 was assumed to be equal to K_3 thereby fixing the value of K_6); in the second iteration, the 9 coefficients of the linear combination of the three U columns were obtained which

* The research was supported in part by MURST grants (40% and 60% to E. C. and 60% to C. S.). The costs of publication of this article were defrayed in part by the payment of page charges. This article must therefore be hereby marked "*advertisement*" in accordance with 18 U.S.C. Section 1734 solely to indicate this fact.

[1] The abbreviations used are: MOPS, 4-morpholinepropanesulfonic acid; BisTris, 2-[bis(2-hydroxyethyl)amino]-2-(hydroxymethyl)-propane-1,3-diol; SVD, singular value decomposition.

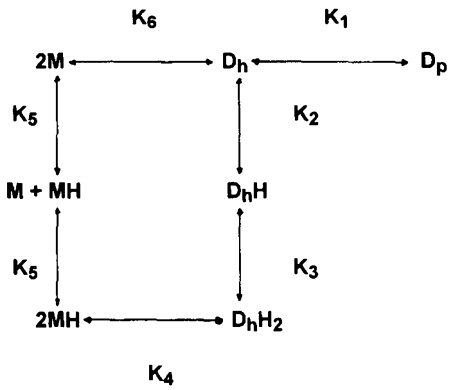

SCHEME I.

yield the best fit to the experimental data. Thus, the estimate of the equilibrium constants and three new basis spectra (nonorthogonal) corresponding to the absorption spectra of the pure species A_{D_h}, A_{D_p}, and A_{MH} have been obtained. In particular, the observed absorption spectrum, A_{obs}, at each pH value is given by:

$$A_{obs} = A_{D_h} + A_{D_p} + A_{MH} = \Sigma_i (C_{i_j} \times U_{n_i})$$

where C_{i_j} represents the (3 × 3) matrix of the linear combination coefficients and U_{n_i} is the (3 × n) matrix containing the first three U columns for n wavelengths. This information can be used to calculate the fraction of the components at every pH value.

RESULTS

Buffer and Ionic Strength Effects—A first set of experiments was carried out at pH 7.0 and at a protein concentration of 5 × 10^{-5} M in order to study specific buffer and ionic strength effects. The optical spectra measured in phosphate, MOPS-NaOH ± Ca^{2+}, BisTris-HCl, and Tris-HCl buffers at an ionic strength of 0.1 M were indistinguishable. In contrast, marked effects of ionic strength were observed in MOPS-NaOH buffer at pH 7.0. Thus, an increase in ionic strength produces a decrease of the high spin bands at about 600 and 630 nm with respect to the low spin ones. Representative spectra at I = 0.01 and 0.1 M are shown in the *inset* of Fig. 1. The change in the relative amounts of high and low spin components with an increase in ionic strength is plotted in Fig. 1 as the difference between the absorbance at 600 and 560 nm, normalized with respect to protein concentration. Fig. 1 also shows that additions of a ferricyanide solution or of concentrated buffer to oxidized HbI in 0.01 M buffer to yield the indicated ionic strength have different effects. Ferricyanide appears to be more effective in stabilizing the low spin species than all the other ions tested.

Effect of pH and Protein Concentration—Several sets of experiments were performed; the effect of pH changes at constant protein concentration and ionic strength was studied first (Fig. 2). Thereafter, the effect of changing the protein concentration at constant pH (in the range 6.5–8.0) and ionic strength (0.01 or 0.1 M) was analyzed. A typical set of data is shown in Fig. 3. In line with the results reported in Fig. 1 and in Ref. 1, the low spin bands (at 526 and 560 nm) dominate the spectrum at acid pH values, low protein concentration, and high ionic strength, whereas the high spin band at 602 nm prevails at alkaline pH, high protein concentration, and low ionic strength. Moreover, the high spin band at 634 nm is visible at neutral and acid pH values.

The spectra of the pH titration (Fig. 2) were analyzed with the singular value decomposition (SVD) procedure in order to single out the contribution of the different components. The three most significant V (*panels a–c*) and U (*panel d*) columns are given in Fig. 4. The linear combination of the first three U columns yields the three basis spectra of Fig. 5, which display

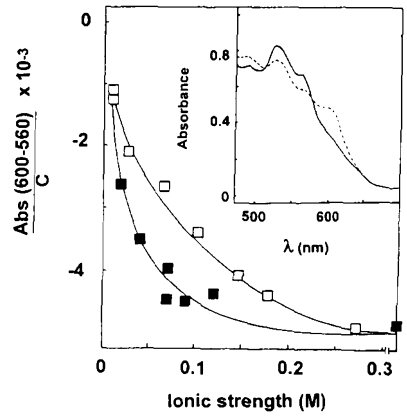

FIG. 1. **Effect of ionic strength on the relative amounts of high spin and low spin components in oxidized HbI at pH 7.0.** Protein concentration, 5 × 10^{-5} M; temperature, 20 °C. Indicated ionic strength obtained with: MOPS-NaOH buffer (□), MOPS-NaOH buffer, I = 0.01 M plus ferricyanide (■). *Inset*: absorption spectra of 5 × 10^{-5} M oxidized HbI in MOPS-NaOH buffer I = 0.01 M (– – –) and 0.1 M (——).

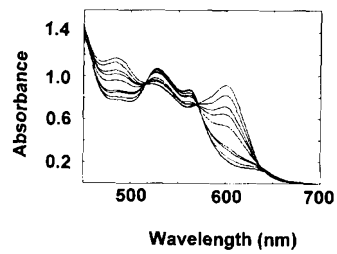

FIG. 2. **Spectrophotometric pH titration of oxidized HbI.** Protein concentration, 5 × 10^{-5} M in MOPS-NaOH buffer, I = 0.01 M, temperature, 20 °C. pH values (from above downward at 602 nm) 8.7, 7.9, 7.6, 7.3, 7.0, 6.65, 6.5, 6.2, 6.0, 5.9, 5.7.

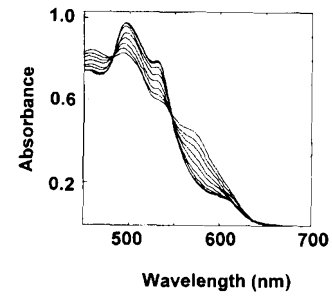

FIG. 3. **Effect of protein concentration on the absorption spectrum of oxidized HbI at pH 6.5.** MOPS-NaOH buffer, I = 0.01 M; temperature, 20 °C. The *top spectrum* at 602 nm corresponds to the initial protein concentration, 5 × 10^{-4} M; the other spectra were obtained upon successive 2-fold dilutions and were normalized to emphasize the changes in lineshape.

the characteristic features of low spin (λ_{max} 526 and 560 nm), aquomet (λ_{max} 634 nm), and pentacoordinate (λ_{max} 602 nm) ferric derivatives. The fraction of the three species at the different pH values, calculated in the same way from the linear combination of the V columns, is given in Fig. 6.

The optical absorption spectra measured at constant pH and ionic strength as a function of protein concentration (*e.g.* the spectra given in Fig. 3) likewise have been analyzed in terms of the three basis spectra in order to obtain the fraction of the different components in solution (Figs. 7 and 8).

A global fit of the data sets of Figs. 7 and 8 to the linkage scheme given under "Materials and Methods," using a least squares procedure, yielded the equilibrium constants listed in Table I. The initial guess of the constants was obtained by fitting the pH titration data.

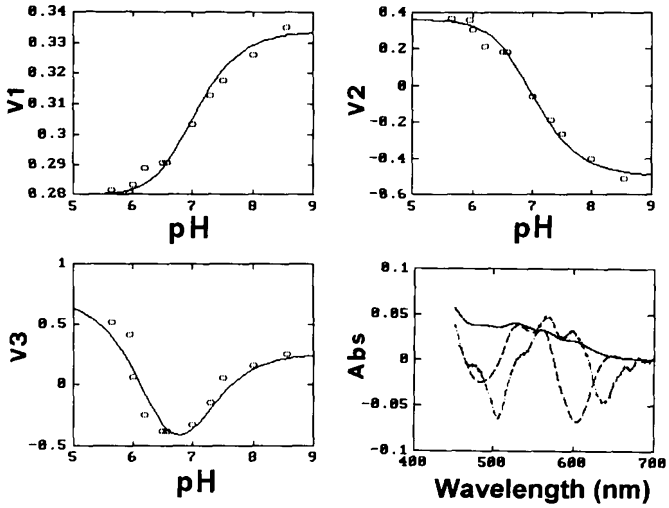

FIG. 4. **SVD analysis of the data matrix of Fig. 2.** *Panels a–c* show the first three V columns and *panel d* the first three U columns: U1 (——), U2 (— — —), U3 (– · –). *Solid lines* in *panels a–c* were calculated using the scheme given under "Materials and Methods."

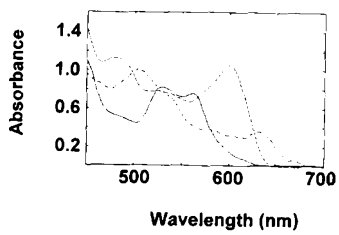

FIG. 5. **Basis spectra obtained from the linear combination of the U columns of Fig. 4.** High spin pentacoordinate (— — —) and hexacoordinate (– · –) species and low spin hemichrome (——).

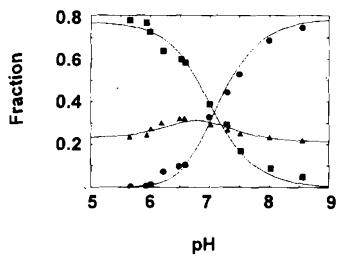

FIG. 6. **Fraction of the high spin and low spin components of oxidized HbI as a function of pH.** Component: high spin pentacoordinate (●), high spin hexacoordinate (▲) heme, low spin hemichrome (■). The fraction of each species was calculated from the data set in Fig. 2 as detailed under "Materials and Methods." *Continuous lines* represent the fit to the linkage scheme given under "Materials and Methods."

Stopped Flow Experiments—Three types of experiment were performed on HbI (3–4 × 10^{-4} M heme) in 0.01 M MOPS-NaOH buffer at pH 7.5. In the first (dilution experiment, Fig. 9*a*), the HbI solution was mixed with the same 0.01 M MOPS-NaOH buffer at pH 7.5; in the second (ionic strength jump, Fig. 9*b*), the protein solution was mixed with 0.2 M MOPS-NaOH buffer at pH 7.5; in the third (pH jump, Fig. 9*c*), HbI was mixed with 0.01 M MOPS-NaOH, pH 6.0, to give a final pH of 6.5. Under all conditions, the spectral transition was followed at 610 nm. The time course corresponds closely to a first order process characterized by a rate constant of 52–57 s^{-1}. Whereas the kinetic absorbance changes correspond to the static one in the dilution and ionic strength jump experiments (A = 0.004 and 0.37, respectively), the kinetic change is significantly smaller than the static change in the pH jump experiment (A = 0.052 *versus* 0.076).

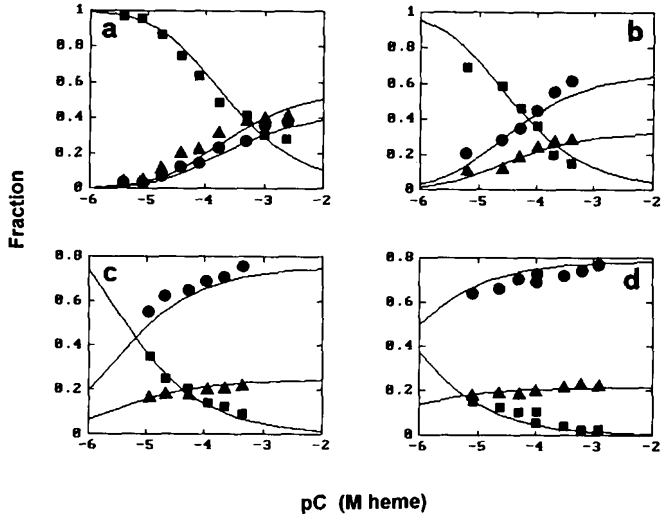

FIG. 7. **Fraction of the high spin and low spin components of oxidized HbI as a function of protein concentration at 0.01 M ionic strength.** MOPS-NaOH buffer, at the indicated pH values. *Symbols* as in Fig. 6.

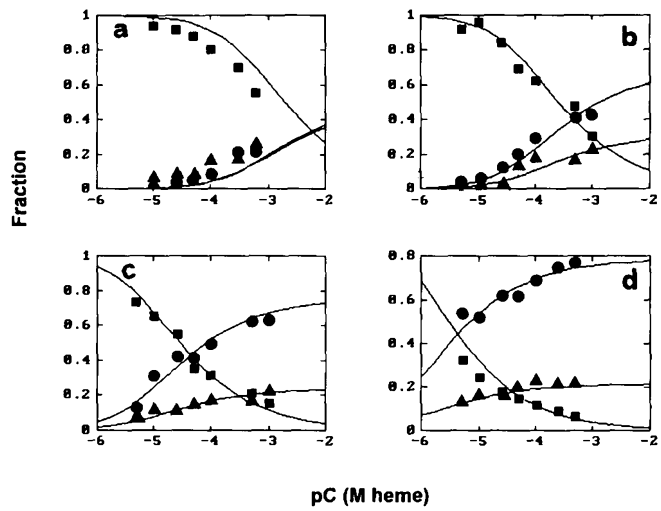

FIG. 8. **Fraction of the high spin and low spin components of oxidized HbI as a function of protein concentration at 0.1 M ionic strength.** MOPS-NaOH buffer, at the indicated pH values. *Symbols* as in Fig. 6.

TABLE I

Equilibrium constants relating subunit dissociation and protonation in oxidized HbI at 0.01 and 0.1 M ionic strength

The equilibrium constants were obtained by fitting the data sets of Figs. 7 and 8 to the linkage scheme presented under "Materials and Methods."

	Ionic strength	
	0.1 M	0.01 M
K_1	0.22	0.15
K_2 (M^{-1})	5.5×10^7	5.5×10^7
K_3 (M^{-1})	1.0×10^5	1.0×10^5
K_4 (M^{-1})	3	20
K_5 (M^{-1})	1.0×10^5	1.0×10^5
K_6 (M^{-1})	1.7×10^3	1.2×10^4

Sedimentation Velocity Experiments—In order to establish whether the high to low spin transition is linked to dissociation into monomers under all experimental conditions, sedimentation velocity experiments have been carried out. This relationship has been established conclusively for the spin transition attendant upon a pH change (1).

The stabilization of the low spin species obtained with an

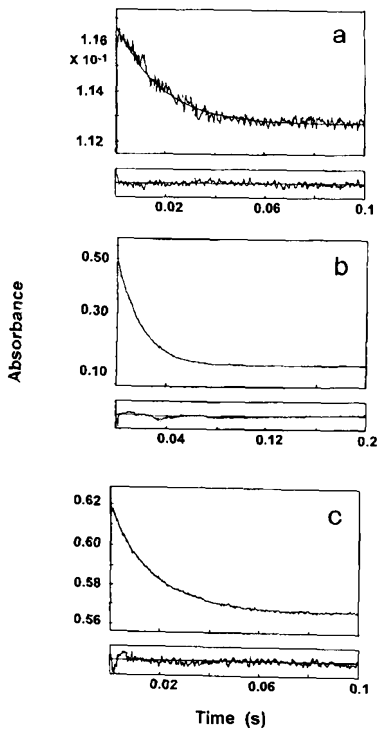

FIG. 9. **Time course of the absorbance change obtained upon dilution of oxidized HbI in rapid mixing experiments.** Hemoglobin solution, 3–4 × 10^{-4} M, in MOPS-NaOH buffer of I = 0.01 M at pH 7.5 diluted 1:1 with the same buffer (*a*); MOPS-NaOH buffer of I = 0.2 M at the same pH (ionic strength jump) (*b*); MOPS-NaOH buffer of I = 0.01 and pH 6.0 yielding a final pH of 6.5 (pH jump) (*c*). Temperature, 20 °C.

increase in ionic strength from 0.01 to 0.1 M at pH 7.0 is indeed accompanied by dissociation as indicated by the s_{20} value of a 2.5 × 10^{-4} M HbI solution which decreases from 2.76 S to 2.15 S.

DISCUSSION

The structural characterization of ferric HbI by means of resonance Raman and EPR spectroscopy has enabled the identification of three distinct heme environments and the assignment of the corresponding optical absorption bands. Thus, the absorption maximum at 634 nm pertains to a high spin aquomet derivative, the bands at 560 and 526 nm to a low spin bis-imidazole heme, and the band at 602 nm to a pentacoordinate heme (2). In turn, recognition that ferric HbI forms two spectrally distinct high spin dimeric species requires a modification of the previously proposed scheme (1) which links the high spin to low spin transition to the pH-dependent monomerization process. In the new scheme which takes the pentacoordinate species into account (see "Materials and Methods"), a simplifying assumption has been made for practical reasons. In order to diminish the number of parameters to evaluate, it has been assumed that the pentacoordinate derivative, which dominates the experimental picture in the alkaline range, is formed only by the deprotonated aquomet derivative.

The simplest possible analysis of the spectral changes in terms of the new linkage scheme rests on the assumption that the protonation steps are spectroscopically silent, *i.e.* that only three spectrally distinct species suffice to describe the system. Within this set of constraints, the observed lineshapes have been deconvoluted using the SVD analysis in order to obtain the spectra of the pure components. The fit of the data set given in Fig. 2 yields three basis spectra (Fig. 5) which do indeed correspond to those of pure high spin aquomet, high spin pentacoordinate, and low spin bis-imidazole heme derivatives, thus validating the assumptions made. In fact, one of the spectra displays peaks at positions and with the relative intensity typical of aquomethemoglobin derivatives in which band III occurs at 633 nm, band IV appears as a broad peak at 580 nm, and the Q_o and Q_v bands are centered at 540 and 500 nm, respectively (7). The other two basis spectra correspond to those of the pentacoordinate 2-Me-imidazole-Fe-protoporphyrin IX complex (8) and of the distorted iron-bis-imidazole derivative (9).

The spectra of the pure species derived from the SVD analysis were used for a global fit of the data sets in Figs. 2, 7, and 8 to the linkage scheme. The agreement between the theoretical and measured optical absorption changes is good. A deviation from the theoretical prediction is observed only at pH 6.5 and high ionic strength, namely under conditions where the measured absorbance changes are small and hence the experimental error is relatively large.

The values of the equilibrium constants describing the system at the two ionic strengths studied are presented in Table I. The protonation and dissociation constants at the higher ionic strength cannot be compared directly with those of Ref. 1 due to the different linkage scheme employed. However, a necessary requirement to describe the experimental data still is the cooperative binding of protons to dimers, which therefore must undergo a proton-linked structural change. This property has been ascribed to the aquomet derivative, since the simplifying assumption has been made that the pentacoordinate component does not bind protons. The extension of the scheme to include the pentacoordinate derivative is reflected mainly in the decrease of the dissociation constant of protonated aquomet dimers. A further difference concerns the protonation constant of monomers, K_5, which has been made equal to K_3 (1 × 10^5 M^{-1}) rather than to K_2 (5.5 × 10^5 M^{-1}) for the reasons given below.

The influence of ionic strength on subunit dissociation in the range 0.01–0.1 M points to the existence of specific ion effects and is in marked contrast with the stability of the reduced protein which does not dissociate up to 2 M ionic strength (4). The effect of ferricyanide depicted in Fig. 1 suggests that anion binding may contribute to destabilize the interface of the ferric protein. The change in ionic strength leaves the protonation constants unaltered, as expected for a process that depends solely on the state of association of the protein.

The stopped flow measurements provide information on the dynamics of the system, in particular on the rates of the $D_p \leftrightarrow D_h$ transition. When the equilibrium is perturbed, be it by changes in protein concentration, pH, or ionic strength (Fig. 9, *a–c*), re-equilibration takes place at about 55 s^{-1} which corresponds to the rate of dimer dissociation (1). It follows that not only the protonation step, but also the $D_p \leftrightarrow D_h$ transition is fast. Accordingly, in the pH-jump experiments, the $D_p \leftrightarrow D_h \leftrightarrow D_hH \leftrightarrow D_hH_2$ relaxation occurs in the dead time of the apparatus (3 ms), and the kinetic absorbance change is smaller than the static one (Fig. 9*c*). Moreover, in the experiments carried out at constant pH (ionic strength jump or 1:1 dilution), where the dimerization equilibrium is perturbed directly and the whole relaxation process is limited by the dissociation rate, the static and kinetic absorbance changes are identical.

In the absence of a crystal structure of ferric HbI, any molecular description of the system has to rest on the crystallographic data of the ferrous derivatives (10, 11). However, the different stability of the dimeric assembly in the two oxidation states indicates that oxidation-linked and oxygenation-linked structural changes must differ significantly from one another. It may be envisaged that the decreased stability of the ferric protein toward dissociation is accompanied by significant changes in the heme environment since the heme-carrying E and F helices are involved in the intersubunit contact. On the

distal side, the network of interactions between the near neighbors of the distal histidine (His^{69}, E6) and residues in the F helix of the contralateral subunit is likely to be disrupted. On the proximal side, other interactions may be affected, *e.g.* those linking one of the heme propionates to Lys^{96} (F9) and Asn^{100} (F13), 2 residues located in the last turns of the F helix near the proximal His^{101}. As a matter of fact, the bond between Lys^{96} and the heme propionate provides one of the two hydrogen bonds across the interface, the other being formed by Lys^{30} (B2) and Asp^{89} (F2). The carboxylates involved in these hydrogen bonds will necessarily have a different pK value depending on the state of association of the protein. In particular, a pK of 4–5 may be expected for the free carboxylate in the monomeric protein, and a higher one, *e.g.* 7–7.5, for the hydrogen-bonded carboxylate in the dimer. These considerations provide the rationale for the choice of the pK value for the protonation of monomers. In turn, the value chosen corresponds to the protonation of D_hH, the aquomet species in which the proton-linked structural change has already occurred. The carboxylates of the heme propionate and of Asp^{89} are the obvious candidates responsible for the monomerization-protonation linkage as they are the only groups at the subunit interface which ionize in the appropriate pH range. Deprotonation of the proximal histidine N_δH cannot be ruled out, although its pK is unknown and its linkage to the state of association of the protein would be indirect. The discrimination between these candidates requires additional information that necessitates the use of modifed hemes or proteins obtained by site-directed mutagenesis.

Lastly, the striking tendency of the aquomet derivative to loose the heme-bound water molecule (Fig. 6) deserves a comment. The loss of water transforms aquomet-HbI into different derivatives, the low spin hemichrome at acid pH values and the pentacoordinate species in the neutral and slightly alkaline pH range, whereas the ionization of the heme-bound water has been detected at pH values above 9 (2). Pentacoordinate hemes have been observed in other hemeproteins (8, 12–14), but their formation has not been correlated to specific structural features of the heme pocket. It is tempting to ascribe the high stability of the pentacoordinate heme in HbI to proximal effects. Thus, a strain in the Fe-His bond could be invoked to explain the anisotropy of the low spin hexacoordinate derivative EPR signal (2) and the optical absorption spectrum of the pentacoordinate species which resembles that of the strained 2-Me-imidazole-Fe-protoporphyrin IX derivative (8). On the other hand ferrous HbI, in both the unliganded and liganded state, is characterized by a reduced covalency of the Fe-His bond as indicated by a number of spectroscopic properties. In deoxy-HbI, the proximal strain manifests itself for example in the low frequency of the Fe-His stretching mode (15), in the small hyperfine shift of N_δH proton resonance (16), and in the highly anisotropic EPR signal of the CO-substituted protein (17). In the CO-liganded protein there is one property, namely the stretching frequency of the Fe-CO bond which is much higher (517 cm^{-1}) than in other hemoglobins and myoglobins, a finding that is generally interpreted as an indication of proximal strain (15, 18). It appears therefore that in HbI, possibly due to the packing of Phe^{97} against the heme and the proximal histidine, in some forms of the protein proximal strain effects are larger than in vertebrate hemoglobins.

Acknowledgment—We thank Dr. Paola Vecchini for carrying out the sedimentation velocity experiments.

REFERENCES

1. Spagnuolo, C., Ascoli, F., Chiancone, E., Vecchini, P., and Antonini, E. (1983) *J. Mol. Biol.* **164,** 627–644
2. Boffi, A., Spagnuolo, C., Chiancone, E., Takahashi, S., and Rousseau, D. L. (1994) *J. Biol. Chem.* **269,** 20437–20440
3. Boffi, A., Bonaventura, C., Bonaventura, J., Cashon, R., and Chiancone, E. (1991) *J. Biol. Chem.* **266,** 17898–17903
4. Chiancone, E., Vecchini, P. Verzili, D., Ascoli, F., and Antonini, E. (1981) *J. Mol. Biol.* **152,** 577–592
5. Spagnuolo, C., Rinelli, P., Coletta, M., Vecchini, P., Chiancone, E., and Ascoli, F. (1988) *Biochim. Biophys. Acta* **956,** 119–126
6. Henry, E. H., and Hofrichter, J. (1992) *Methods Enzymol.* **210,** 129–155
7. Eaton, W. A., and Hofrichter, J. (1976) *Methods Enzymol.* **76,** 175–225
8. Spiro, T. G., and Burke, M. J. (1976) *J. Am. Chem. Soc.* **98,** 5482–5489
9. Salerno, J. C., and Leigh, J. S. (1984) *J. Am. Chem. Soc.* **106,** 2156–2159
10. Royer, W. E., Jr., Hendrickson, W. E., and Chiancone, E. (1989) *J. Biol. Chem.* **264,** 21052–21061
11. Royer, W. E., Jr., Hendrickson, W. E., and Chiancone, E. (1990) *Science* **249,** 518–521
12. Rousseau, D. L., Ching, Y., Brunori, M., and Giacometti, G. M. (1989) *J. Biol. Chem.* **264,** 7878–7881
13. Spiro, T. G., Stong, J. D., and Stein, W. A. (1979) *J. Am. Chem. Soc.* **101,** 2648–2655
14. Rakshit, G., and Spiro, T. G. (1974) *Biochemistry* **13,** 5317–5323
15. Song, S., Boffi, A., Chiancone, E., and Rousseau, D. L. (1993) *Biochemistry* **32,** 6330–6336
16. Inubushi, T., Yonetani, T., and Chiancone, E. (1988) *FEBS Lett.* **235,** 87–92
17. Verzili, D., Santucci, R., Ikeda-Saito, M., Chiancone, E., Ascoli, F., Yonetani, T., and Antonini, E. (1982) *Biochim. Biophys. Acta* **704,** 215–220
18. Yu, N. T., Kerr, E. A., Ward, B., and Chang, C. K. (1983) *Biochemistry* **22,** 4534–4540